JOURNAL OF MATERIALS SCIENCE 27 (1992) 4639–4646

Experimental assessment of modified statistical theory of sintering

TSANG-TSE FANG, H. L. HSIEH
Department of Materials Engineering, National Cheng Kung University, Tainan, Taiwan 70101

Several experiments have been conducted to measure the parameters of microstructural evolution, i.e. pore size, grain size, total length per unit volume of pore, and pore-size distribution. The modified statistical theory of sintering has been employed to evaluate these parameters. The comparisons of experimental and theoretical data are in good agreement, which further justifies the modified statistical theory of sintering. The evaluated activation energy is 1461 kJ mol^{-1} suggesting that Ti^{4+} might be the most probable rate-limiting species in the later stages of sintering of high-purity barium titanate. The morphological parameter, x, which could predict pore shrinkage when $x < 1$ and pore growth when $x > 1$ has further been verified. Surface diffusion might play a role in pore growth and in reducing the total length per unit volume of pore at the beginning of the intermediate stage of sintering. A morphological path for sintering based on the calculated values of microstructural evolution has been proposed, which has been successfully used to sinter high-purity barium titanate to relative density $> 99.4\%$ ρ_t with a fine-grain size of 1.2 μm.

1. Introduction

The properties of fabricated ceramics are essentially determined by the microstructures. For ceramic processing, the sintering processes play the most important role in controlling the microstructure. For a long time, most sintering theories [1–5] have been based on the ideal geometric model, and which though providing a useful measure of various sintering mechanisms, were of little help in fabricating good ceramics. In sintering powder compacts, the morphologies of grains and pores should be taken into account. A basic thermodynamic concept, i.e. pore coordination number, about the pore shrinkage and growth in a powder compact has been proposed and extensively studied [6–9], in which the pore surface would become concave (wherein pores will shrink) or convex (wherein pores will grow) when its coordination number is smaller or larger than the critical one. Rearrangement [10] is significant in a loose compact. For a pressed compact, microstresses might develop [11] which, however, could be relieved by the change of grain morphology during the later stages of sintering [12]. Therefore, this phenomenon is neglected in modelling the later stages of sintering.

Several phenomenological theories about sintering a powder compact have been reviewed by Exner [13]. Among them, Coble's model [14] was widely referenced, and indeed, successful in evaluating the sintering behaviour of numerous materials. However, his geometric model deviates greatly from the real situation of a powder compact and the empirical grain-growth law was employed, which did not take into account the relation between grain size, pore size, and density. To overcome the limitation of Coble's model, Kuczynski [15–19] developed a statistical sintering theory. However, some of the assumptions are still unrealistic, and have been modified by Fang and Palmour [20]. Although a certain amount of evidence has supported this modified theory [21, 22], direct justification is still lacking. The objective of this paper is to provide more experimental data to assess the modified model.

2. Experimental procedure

A barium titanate powder prepared by coprecipitation with a purity $>99.98\%$ and stoichiometry Ba/Ti = 0.999 determined by X-ray fluorescence analysis, was used in this study. The chemical composition analysed by various methods is summarized in Table I. The powders were calcined at 900 °C for 6 h, and then were wet-milled in a jar, made of Nylon 6 plastics, with ZrO_2 balls for 4 h. Ethyl alcohol was used as an effective medium. The contamination was examined by weighing the weight loss of ZrO_2 balls.

TABLE I Chemical composition of as-received powder

Constituent	Analysis method[a]	Concentration
Ba	Wet chemical	58.39 wt %
Ti	Wet chemical	20.39 wt%
Na	AAS	4 p.p.m.
K	AAS	ND[b]
Ca	ICP	ND
Mg	ICP	ND
Sr	Wet chemical	ND
Fe	ICP	ND

[a] AAS, atomic absorption spectrometry; ICP, inductively coupled plasma.
[b] ND, not detected.

0022–2461

The contamination was estimated to be less than 70 p.p.m. After milling, the slurry was wet-pressed in a steel die at 160 MPa, in which no binder or lubricant was used. The disc-shaped specimen was 12 mm diameter and 2 mm thick. Green compacts were dried in an oven at 120 °C for 24 h, and sintering was carried out at temperatures from 1200–1375 °C in air at different rates of 5, 10, and 20 °C min^{-1} without soaking.

The particle morphology of powders after milling was observed by SEM and the particles for SEM observation were prepared by drying a droplet of suspension on a specimen holder in air. The particle-size distribution was determined by a gravitational X-ray sedimentation method. X-ray line-broadening measurement was employed to determine the crystallite size. Green density was measured by the geometric method, and the sintered density was measured by Archimedes' method with distilled, deionized water as the fluid medium. The value of 6.02 g cm^{-3} was used as the theoretical density, ρ_t.

Pore-size distribution was measured by mercury porosimetry. For measurements, the pressure was increased to 366 MPa in 105 steps, the final pressure corresponds to a pore diameter of 3.5 nm. At each step, the pressure was held for 5 s beyond the time at which no further change in pressure was observed. The percentage of the maximum intrusion (STEM) volume used in these measurements was between 40% and 80%. To calculate the pore-size distribution, a mercury surface tension of 485 dyn cm^{-2} and a contact angle of 130° were used.

SEM was employed to observe the fracture surfaces of both green compacts and polished and etched sections of the sintered bodies. Polished sections were prepared by light mechanical grinding followed by a vibratory polishing machine using 1 μm diamond paste. Grain boundaries were revealed by thermal etching. The average grain size was measured by a computer using an image analyser, and more than 600 grains were averaged.

3. Results and discussion

3.1. Characterization of powders and green compacts

Fig. 1 shows the particle-size distribution of calcined powders after milling. As observed, the particle-size distribution is narrow and the average particle size is 0.92 μm. Fig. 2 shows the particle morphology of the milled powders. It is seen that the particle size and shape are very uniform. Moreover, the detail of the substructure of the milled powders was examined using a higher magnification scanning electron micrograph (Fig. 2b). As observed, the powders consist of a few partially sintered fine particles. X-ray line-broadening diffraction measurement shows that the crystallite size of these powders is 23 nm. Fig. 3 shows the fracture surface of the green compact. The observed microstructure is very uniform. Fig. 4 shows that the pore size distribution of the green compact is narrow. The average pore diameter is 92 nm.

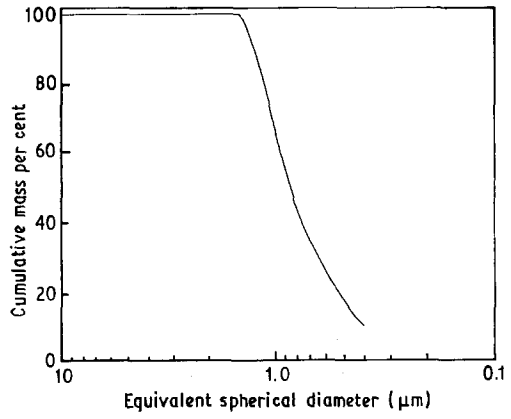

Figure 1 Particle-size distribution of calcined powders after milling.

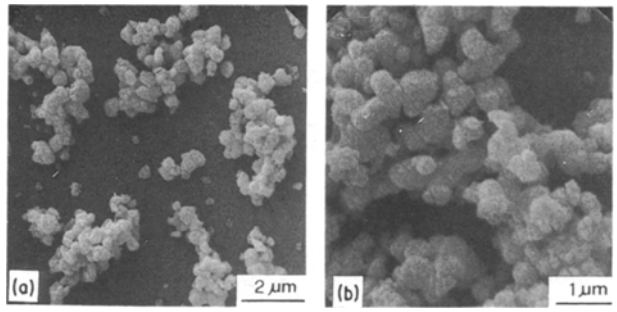

Figure 2 (a) Particle morphology of milled powders and (b) high magnification scanning electron micrograph showing detail of substructure of milled powders.

3.2. Sintering behaviour

Fig. 5 shows the sintering behaviour of the high-purity barium titanate at different heating rates. The densification rate is increased as the heating rate increases. In evaluating the activation energy for sintering high-purity barium titanate, the modified statistical theory of sintering [20] will be employed, which has successfully interpreted the sintering behaviour of high-purity alumina powder compacts [21, 22]. In this modified model, pore coordination number was adopted to take into account of pore shrinkage and growth, and Zener's relationship was introduced to relate the grain

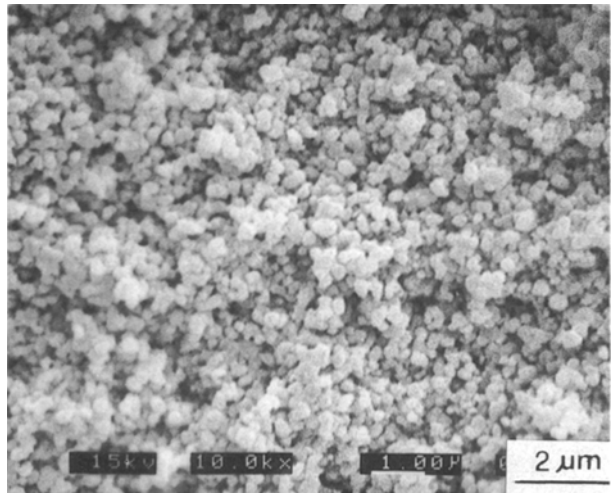

Figure 3 Scanning electron micrograph of the fracture surface of a powder compact.

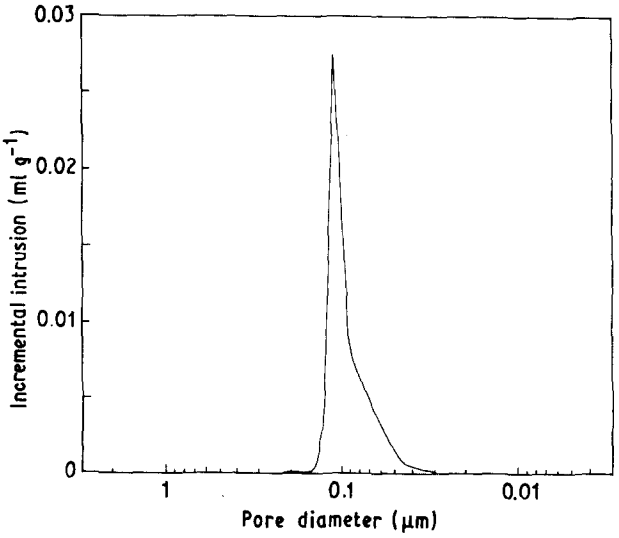

Figure 4 Pore-size distribution of a powder compact.

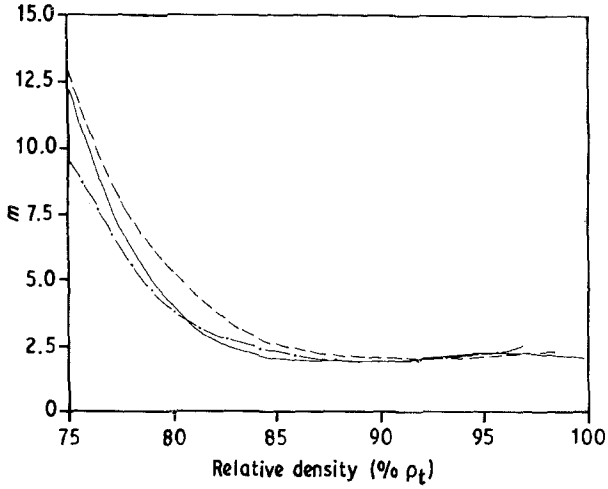

Figure 6 Values of m as a function of relative density for samples sintered at (——) 10 °C min^{-1}, (– – –) 5 °C min^{-1}, (—·—) 20 °C min^{-1}.

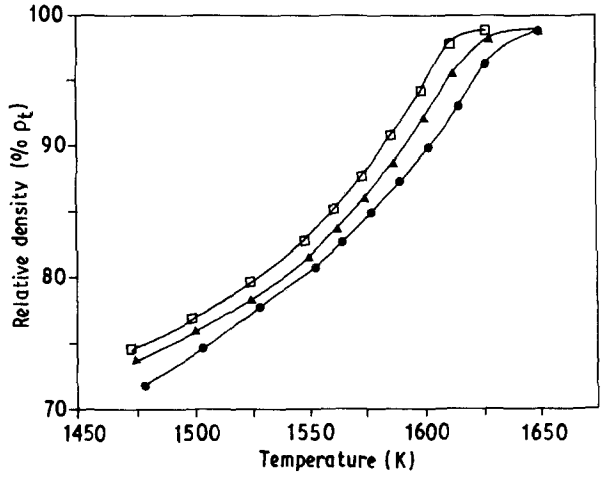

Figure 5 Relative density versus sintering temperature for samples sintered at (●) 20 °C min^{-1}, (▲) 10 °C min^{-1}, (□) 5 °C min^{-1}.

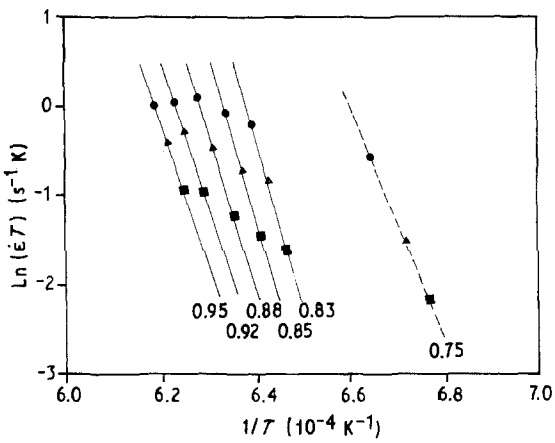

Figure 7 The natural logarithm of $\dot{\varepsilon}T$ as a function of $1/T$ for the relative densities of 0.75, 0.83, 0.85, 0.88, 0.92 and 0.95, at (●) 20 °C min^{-1}, (▲) 10 °C min^{-1}, (■) 5 °C min^{-1}. The average slope yields an activation energy of 1461 kJ mol^{-1}.

growth with pore morphology. The morphological kinetic equation, developed for evaluating the activation energy and microstructural evolution, may be rewritten in the form

$$\ln(\dot{\varepsilon}T) = \ln[(\gamma/k)D^*A_iF_i(y, Z)(p/p_0)^{m_i}] + (-Q/R)(1/T) \quad i/1, 2 \qquad (1)$$

where $\dot{\varepsilon}$ is the densification rate, D^* the diffusion constant, γ the surface energy, Q the activation energy, and k (J K^{-1}) [or R (J mol^{-1} K^{-1})] is Boltzmann's constant. The intercept parameter, A, is a function of the initial condition of each stage, while the morphological terms, m and y, are related to morphological parameter, x, and pore-size distribution, respectively. Z represents the fraction of active (i.e. shrinking) pores. The subscripts, 1 and 2, represent the intermediate and final stages of sintering, respectively.

Because the difference of the morphological parameters (y, Z, and m) in the first term on the right-hand side of Equation 1 is small at the same density level for different heating rates when relative density, D, >0.825, as seen in Fig. 6, and thus, they could be assumed to be constant, especially when taken logarithmically. As observed in Fig. 7, the data points for different heating rates were situated at the same line at each density level. Moreover, these lines are parallel, which further suggests that there is a single mechanism dominating in the later stages of sintering of high-purity barium titanate. The line of $D = 0.75$, indicated by a dashed line, deviates slightly from other lines and might be due to the growth of pores through surface diffusion, which influences the morphological parameters and is significant for the low heating rate. The calculated value of activation energy, 1461 kJ mol^{-1}, is consistent with the theoretical value reported by Lewis *et al.* [23] which suggests that titanium ions might be the most probable rate-limiting species in the later stages of sintering of high-purity barium titanate. However, on the basis of the calculated activation energy value, the estimated value of D^* calculated from Equation 1 is too large, but the diffusivity (10^{-10} cm^2 s^{-1}) is reasonably in agreement with the creep data [24]. Moreover, the creep studies of the titanate materials [25, 26] also showed high creep rate with high activation energy. This interesting phenomenon might be the reason why no diffusivity data of Ti^{4+} in barium titanate is available so far.

3.3. Comparisons of experimental and theoretical data of microstructural evolution

The theoretical values of the parameters of the microstructural evolution, pore size, $\bar{r}$, grain size, $\bar{a}$, total length per unit volume of pore, L_v, and pore-size distribution, cannot be determined until the onset points of the later stages of sintering are known. The procedure for determining these points has been detailed in the previous work [21]. Following the procedure, the determined onset relative densities of the intermediate and final stages are 0.7 and 0.92, respectively, as shown in Fig. 8. It should be noted that only the samples sintered at 10 °C min^{-1} were selected for comparison of the experimental and evaluated parameters of microstructural evolution. Because the pore size and its distributions in the final stage are difficult to measure with our facility, comparison of the theoretical and experimental data was omitted. The m values in Equation 1 could be obtained from the slope of

$$\ln(\dot{\varepsilon}T) + (Q/R)(1/T) = \ln[(\gamma/k)D^*A_iF_i(y,Z)] + m_i \ln(p/p_0) \quad i/1,2 \quad (2)$$

It should be noted that Equation 2 is assumed to be linear over a very short time interval, as discussed in the previous work [21]. The corresponding values of x can be calculated directly from the relationships established in the preceding paper [21]: $m_1 = 3x_1$ and $m_2 = 2 + x_2$. However, these relations will be changed, if the exponent s in Zener's equation ($\bar{a} = k\bar{r}/p^s$, where $\bar{a}$ is the grain size, $\bar{r}$ the pore size, and p the porosity) is altered. The theoretical values of s are 1/2 and 1 for the intermediate and final stages of sintering, respectively.

The experimental results in Fig. 9 showing that the s value is 0.7, suggest that the theoretical s value (0.5) is valid. For the final stage of sintering, it has been shown [27] that most pores are located at the grain edges or corners. In such a case, Saetre *et al.* [28] have shown that $s = 1$, i.e. $\bar{a} = k\bar{r}/p$ is still a good approximation. However, Hillert [29] proposed that $s = 0.93$ is more correct for $p < 0.1$, so $s = 0.9$ is also selected for comparison. The relationships between m and

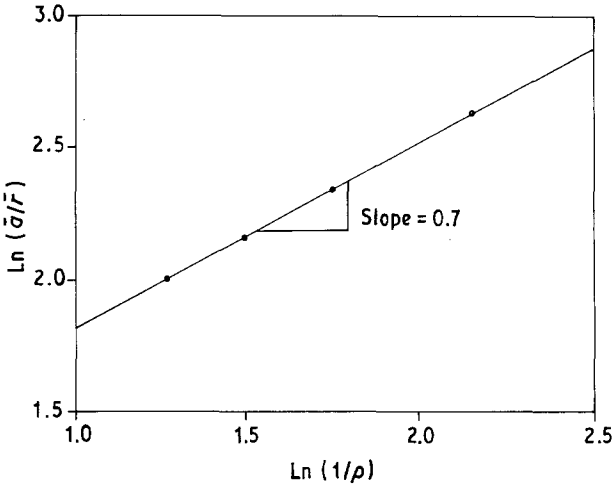

Figure 9 The experimental result of Zener's relationship in the intermediate stage of sintering showing that $s = 0.7$.

x will be changed: $m_1 = 3x_1 + 0.4$ ($s = 0.7$) and $m_2 = 1.8 + x_2$ ($s = 0.9$). As observed in Fig. 10, the x values begin at >1 and drop to <1 when relative densities >0.8, i.e. pores grow at the beginning and begin to shrink at relative densities higher than 0.8 for $s = 0.7$ and 0.82 for $s = 0.5$, which is reasonably consistent with the experimental data in Fig. 11 showing

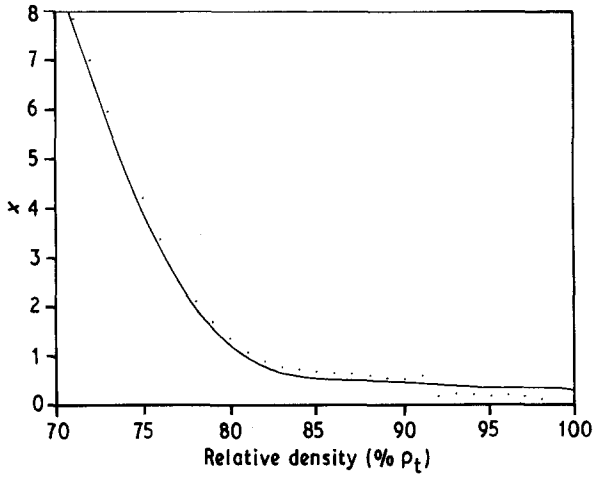

Figure 10 Morphological parameter x as a function of relative density for the specimen sintered at 10 °C min^{-1}. (· · ·) x ($s = 0.5$, 1.0), (——) x' ($s = 0.7$, 0.9).

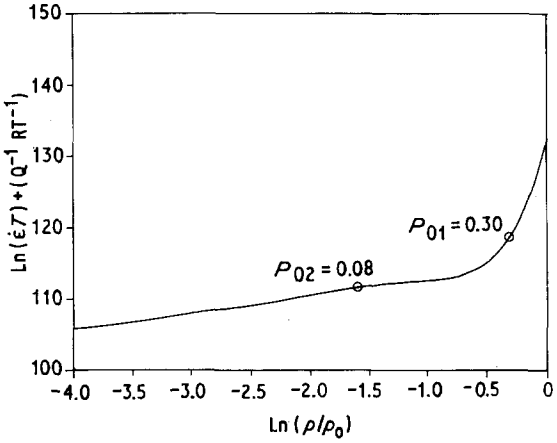

Figure 8 Logarithm of normalized densification rate versus logarithm of normalized porosity for the specimen sintered at 10 °C min^{-1}. p_{01} and p_{02} indicate the onset points of the intermediate and final stages of sintering, respectively.

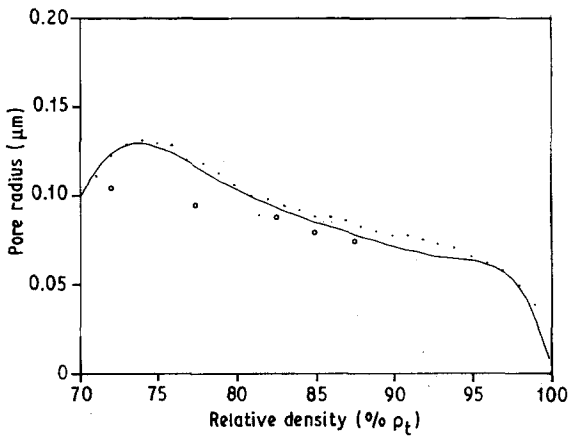

Figure 11 Comparison of (○) experimental and (· · ·, —) theoretical data of pore radius as a function of relative density for the specimen sintered at 10 °C min^{-1}. (· · ·) x ($s = 0.5$, 1.0), (——) x' ($s = 0.7$, 0.9).

that pores begin to shrink with relative densities >0.78. It should be noted that the onset relative density of the intermediate stage of sintering is 0.7.

Using the onset relative densities and the calculated values of morphological parameter x, grain size, pore size, total length per unit volume of pore and pore-size distribution could be evaluated [21]. As observed in Fig. 11, the experimental and theoretical data of pore size are in good agreement, and the theoretical data with $s = 0.7$ is more consistent. The theoretical data between relative densities 0.7 and 0.8 deviate a little more from the experimental data, which might be due to the overlapping of the initial and intermediate stages of sintering. As can be seen in Fig. 8, that is a curved region between relative densities 0.7 and 0.8. It should be noted that the pore size of the onset relative density (i.e. 0.92) in the final stage of sintering is estimated from that of the final relative density in the intermediate stage of sintering. The total length per unit volume of pore at a given density could be evaluated by dividing the summarized length, l_i, of each mean pore radius, $\bar{r}_i$, by the total volume of the specimen. The length of each mean pore radius could be calculated by considering the measured increment volume to be a cylinder with a radius, $\bar{r}_i$ (measured), and a length, l_i (unknown). As observed in Fig. 12, the experimental and theoretical data of L_v are in reasonable agreement, and the theoretical data with $s = 0.7$ are more consistent.

Fig. 13 shows the grain size versus relative density. For the intermediate stage of sintering, the experimental and theoretical data are in good agreement, and the theoretical data are also more consistent. For the final stage of sintering, both sets of data are in reasonable agreement, and $s = 0.9$ is a little bit better. The deviation of theoretical data more from the experimental ones when the fractional densities > 0.96 is due to the invalidity of the model as discussed in the previous paper [20]. Inferring from the data shown in Figs 12 and 13, grain growth become slower for high values of L_v. The theoretical y values, assuming $Z = 1$, are shown in Fig. 14, and the values decrease as the relative density decrease, because the standard deviation derived from theory represents the distribution of pore radii, but that of the experiment represents the distribution of pore volume. Therefore, the only way to compare the experimental and theoretical data of the distribution of pore size is to evaluate the probability of different radii. The probability of the theoretical data is calculated by dividing the area of each mean pore radius (wherein the interval is the same as that of the measured data) by the total area under the lognormal distribution curve. The probability of the experimental data is derived by dividing the increment volume of each mean pore radius by the total increment volume. Fig. 15 shows the comparison of the experimental and theoretical data of pore-size distribution (probability versus radii) in the intermediate stage of sintering for three different densities. As observed, the experimental and theoretical data are in reasonable agreement for $s = 0.7$ or 0.5. The agreement of the experimental and theoretical data of the parameters of microstructural evolution further justifies the modified statistical theory of sintering. It is noted that the Equations 30 and 31 in [20] should be

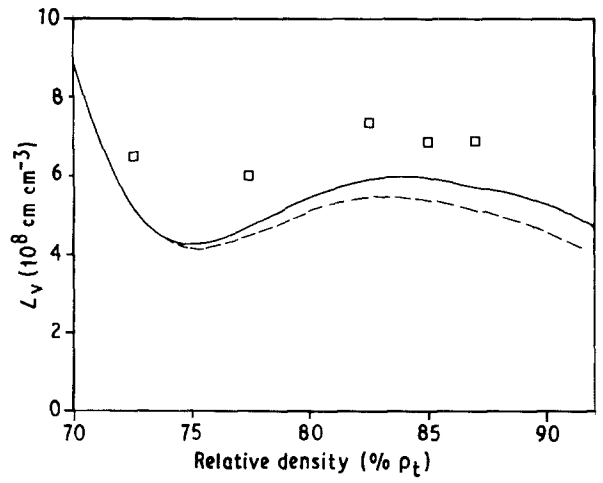

Figure 12 Comparison of (□) experimental and (——, ——) theoretical data of total length of pores per unit volume as a function of relative density for the specimen sintered at 10 °C min^{-1}. (– – –) x ($s = 0.5$, 1.0), (——) x' ($s = 0.7$, 0.9).

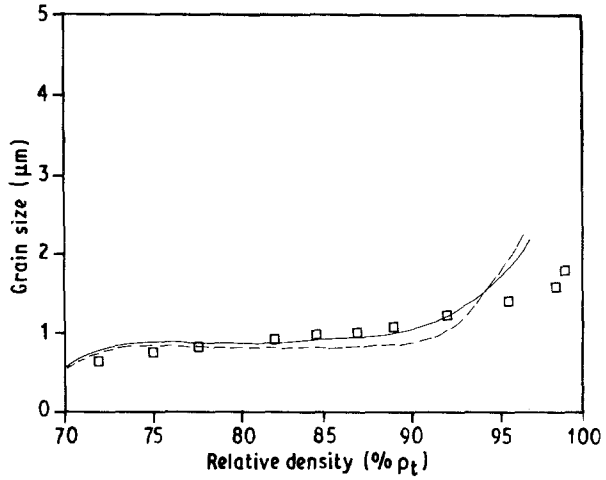

Figure 13 Comparison of (□) experimental and (– – –, ——) theoretical data of grain size–relative density trajections for the specimen sintered at 10 °C min^{-1}. (– – –) x ($s = 0.5$, 1.0), (——) x' ($s = 0.7$, 0.9).

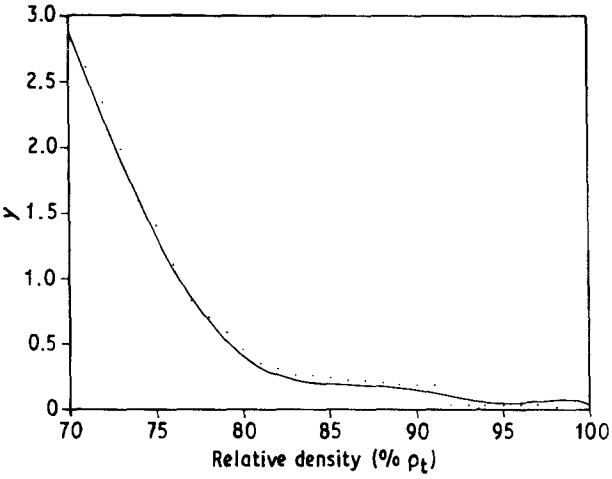

Figure 14 Values of the relative width of the pore size distribution, y, as a function of relative density for the specimen sintered at 10 °C min^{-1}, for (· · ·) x ($s = 0.5$, 1.0), (——) x' ($s = 0.7$, 0.9).

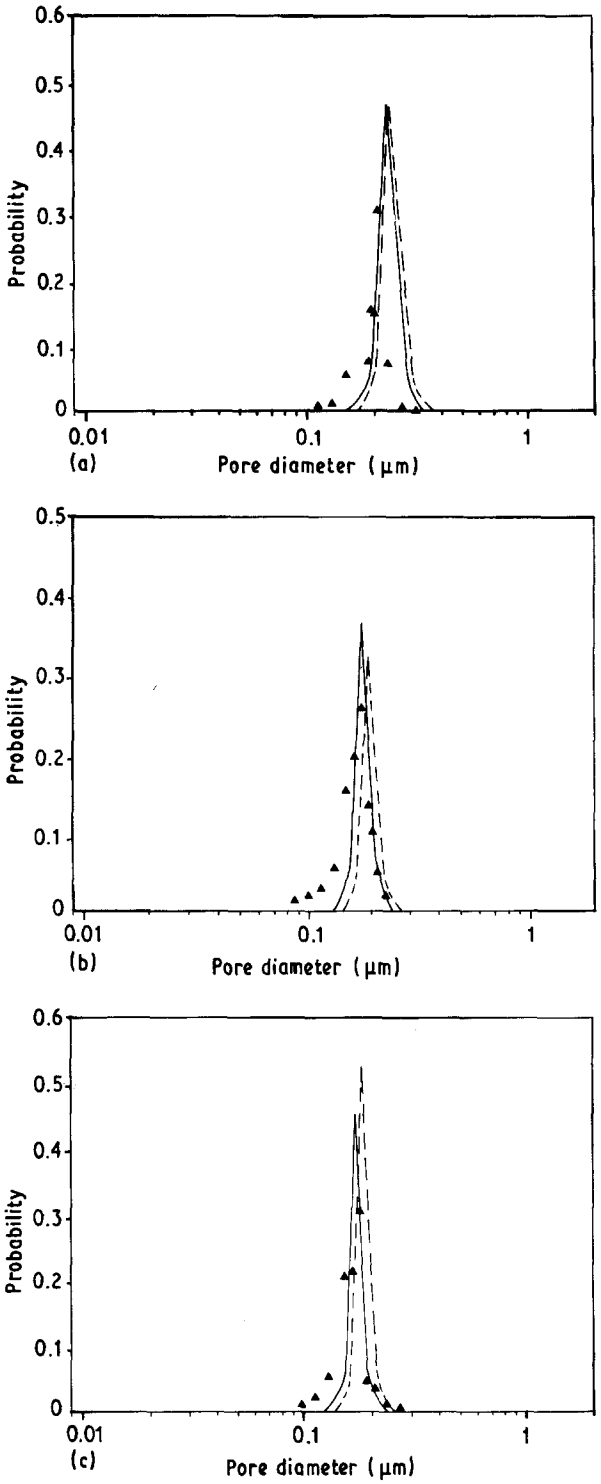

Figure 15 Comparison of (▲) experimental and (– – –, ——) theoretical data of pore-size distributions (probability versus radii) at (a) $D = 0.775$, (b) $D = 0.825$, and (c) $D = 0.846$. (– – –) x ($s = 0.5, 1.0$), (——) x' ($s = 0.7, 0.9$).

corrected to

$$x_1 = \frac{21yZ - 3y + 5yZ + y}{2Z(1 + 3y)} \quad (3)$$

and

$$x_2 = \frac{y(9yZ - 3y + 10yZ + 2y + 5Z + 1)}{Z(1 + y)} \quad (4)$$

3.4. Application of the theory

On evaluating the parameters of the microstructural evolution, it is possible to pave the morphological path for sintering. In previous work [21], the morphological path for sintering alumina has been proposed and successful, but it should be modified due to the fact that some experimental data were not available at that time. The modified profile based on the morphological parameters $\bar{r}$ and L_v at different heating rates (Figs 16 and 17, respectively) has been proposed in Fig. 18. It should be noted that because the onset point of these parameters for different heating rates is different, the values of $D \geqslant 0.75$ were selected for comparison. There are four regions to be discussed. The first region (end point D_1), involves the initial stage and pore-growth region of the intermediate stage of sintering, e.g. the end point of this region for 10 °C min^{-1} should be $D \approx 0.81$ in sintering barium titanate, as shown in Fig. 11. As mentioned above, the surface diffusion dominates and makes pores grow, therefore, a high heating rate should be employed. As observed in Figs 16 and 17, the higher the heating rate, the smaller is the relative pore radius and the larger relative values of L_v at a given density. Thus, a high heating rate not only supresses the surface diffusion but also retains higher values of L_v which, in turn, will have larger drag force to inhibit the grain growth in the second region. It should be pointed out that in previous work [21], the onset point of the

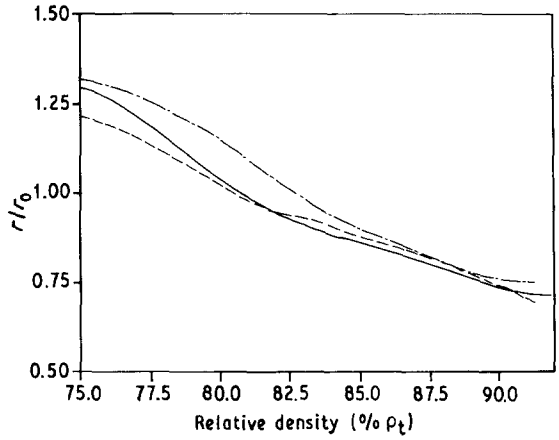

Figure 16 Relative pore radius as a function of relative density for the specimens sintered at (——) 10 °C min^{-1}, (— · —) 5 °C min^{-1}, (– – –) 20 °C min^{-1}.

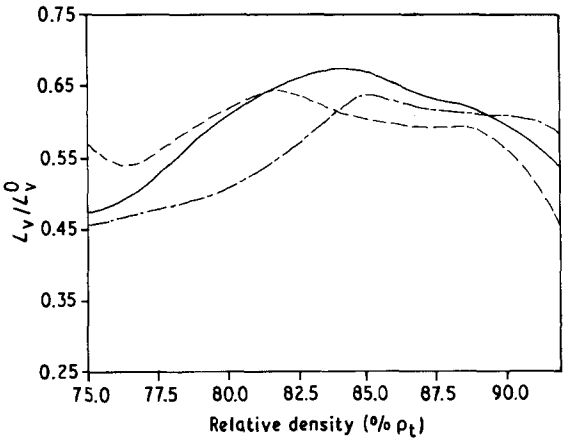

Figure 17 Relative total length of pores per unit volume as a function of relative density for the specimens sintered at (——) 10 °C min^{-1}, (— · —) 5 °C min^{-1}, (– – –) 20 °C min^{-1}.

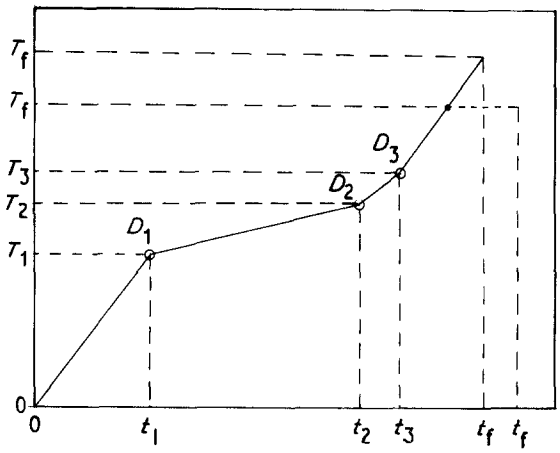

Figure 18 Design of the morphological path for sintering a powder compact based on the data showing in Figs 16 and 17.

intermediate stage of sintering selected as the end point of this region, should be altered.

The end point of the second region, D_2, is selected as L_v begins to decrease quickly. As observed in Fig. 17, the lower the heating rate, the longer it takes to reach the maximum L_v. Therefore, in this region, a lower heating rate should be employed because it will be benefited by maintaining a higher value of L_v, which in turn will lower the grain-growth rate. The third region has end point D_3, which is the onset relative density of the final stage of sintering. Because L_v starts to decrease quickly and the grain-growth rate might be enhanced, it is better to use a medium heating rate. This region was omitted in the previous work [21] but according to this study, it should be retained for an optimal result. The fourth region corresponds to the final stage of sintering. In this region, the grain-growth rate might be higher than the densification rate at lower temperature, therefore, a higher heating rate should be used. The end point of this region is determined by the experiment and is dependent on the material properties. If the anisotropic grain growth of a ceramic is significant, it is better for it to be sintered isothermally at a lower temperature, as shown by the dashed line in Fig. 18. Three specimens having the same green density (≈ 0.60) are sintered using different profiles: (a) 10 °C min^{-1} to 1375 °C without soaking, (b) 10 °C min^{-1} to 1300 °C and soaked for 8 h, and (c) 20 °C min^{-1} to 1265 °C, 2.5 °C min^{-1} to 1300 °C, 5 °C min^{-1} to 1312 °C, and 20 °C min^{-1} to 1350 °C without soaking. The results shown in Fig. 19 are remarkably different. The specimens using constant heating rate and conventional isotherm (Fig. 19a and b) have $D \approx 99\%$ ρ_t with grain size 1.8 and 3.0 μm, respectively. The specimen using the modified profile (Fig. 19) has higher density (99.4% ρ_t) and a more uniform fine-grained (1.2 μm) microstructure.

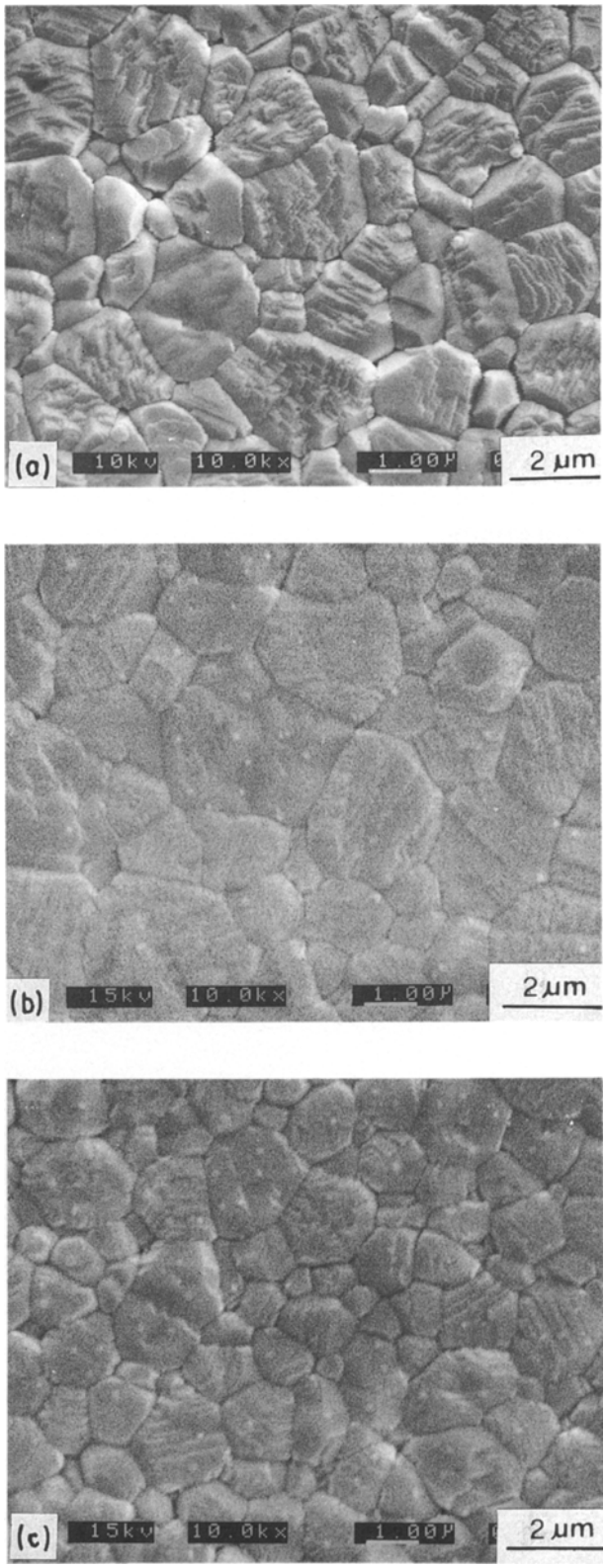

Figure 19 Scanning electron micrographs of the sintered specimens using different profiles: (a) 10 °C min^{-1} to 1375 °C without soaking ($D = 0.99$, $\bar{a} = 1.8$ μm), (b) 10 °C min^{-1} to 1300 °C and soaked for 8 h ($D = 0.991$, $\bar{a} = 3.0$ μm) and (c) 20 °C min^{-1} to 1265 °C, 2.5 °C min^{-1} to 1300 °C, 5 °C min^{-1} to 1312 °C, and 20 °C min^{-1} to 1350 °C without soaking ($D = 0.994$, $\bar{a} = 1.2$ μm).

4. Conclusions

1. The modified statistical theory of sintering has further been proved to be able to evaluate the parameters of microstructural evolution, which are in good agreement with the experimental data.

2. The evaluated activation energy is 1461 kJ mol^{-1}, which suggests that Ti^{4+} might be the most probable rate-limiting species in the later stages of sintering for the high-purity barium titanate.

3. The morphological parameter, x, which could predict pore shrinkage when $x < 1$ and pore growth when $x > 1$ has further been verified.

4. Surface diffusion might play a role in pore growth and in reducing the total length per unit volume of pore at the beginning of the intermediate stage of sintering.

5. Based on the evaluated values of microstructural evolution, it is possible to pave the morphological path for sintering, which has successfully sintered high-purity barium titanate to relative density $> 99.4\%$ ρ_t with a fine-grain size of 1.2 μm.

Acknowledgement

The authors thank the National Science Council for the financial support under Contract no. NSC-77-0405-E006-04.

References

1. G. C. KUCZYNSKI, *Trans. Amer. Inst. Min. (Metall) Eng.* **185** (1949) 169.
2. W. D. KINGERY and M. BERG, *J. Appl. Phys.* **26** (1955) 1205.
3. R. L. COBLE, *J. Amer. Ceram. Soc.* **41** (1958) 55.
4. D. L. JOHNSON and I. B. CUTLER, *ibid.* **46** (1963) 541.
5. F. A. NICHOLS and W. W. MULLINS, *J. Appl. Phys.* **36** (1965) 80.
6. W. D. KINGERY and B. FRANCOIS, in "Sintering and Related Phenomena", edited by G. C. Kuczynski, N. A. Hooton and G. F. Gibbon (Gordon and Breach, New York, 1967) p. 471.
7. F. F. LANGE, *J. Amer. Ceram. Soc.* **67** (1984) 83.
8. B. J. KELLETT and F. F. LANGE, *ibid.* **72** (1989) 725.
9. F. F. LANGE and B. J. KELLETT, *ibid.* **72** (1989) 735.
10. G. PETZEW and H. E. EXNER, *Z. Metallkde* **67** (1976) 611.
11. A. G. EVANS, *J. Amer. Ceram. Soc.* **65** (1982) 497.
12. H. L. HSIEH and T. T. FANG, *ibid.* **73** (1990) 1566.
13. E. EXNER, in "Reviews on Powder Metallurgy and Physical Ceramics", edited by F. V. Lenel (Freund, Tel Aviv, 1979) p. 34.
14. R. L. COBLE, *J. Appl. Phys.* **32** (1961) 787.
15. G. C. KUCZYNSKI, *Sci. Sintering* **9** (1977) 243.
16. *Idem, Mater. Sci. Res.* **10** (1975) 325.
17. *Idem, Z. Metallkde* **67** (1976) 606.
18. *Idem*, in "Ceramic Microstructure-'76", edited by R. M. Fulrath and J. A. Pask (Westview Press, Boulder, CO, 1977) p. 233.
19. *Idem*, in "Materials Science monographs", Vol. 14, edited by D. Kolar, S. Pejovnik and M. M. Ristic (Elsevier, Amsterdam, 1982) p. 37.
20. T. T. FANG and H. PALMOUR III, *Ceram. Int.* **15** (1989) 329.
21. *Idem, ibid.* **16** (1990) 63.
22. *Idem, ibid.* **16** (1990) 1.
23. G. A. LEWIS, C. R. A. CATLAW and R. E. W. CASSELTON, *J. Amer. Ceram. Soc.* **68** (1985) 555.
24. G. M. DYNNA and Y. M. CHIANG, in "Sintering of Advanced ceramics", Ceramic Transaction, Vol. 7, edited by C. A. Handwerker, J. E. Blendell and W. A. Kaysser (The American Ceramic Society, Westerville, OH, 1990) p. 547.
25. H. YAMADA, *J. Mater. Sci.* **19** (1984) 2639.
26. C. CARRY and A. MOCELLIN, *J. Amer. Ceram. Soc.* **69** (1986) C-215.
27. T. T. FANG, *J. Mater. Sci. Lett.* **7** (1988) 1068.
28. T. O. SAETRE, N. RYUM and O. HUNDERI, *Mater. Sci. Engng* **A108** (1989) 33.
29. M. HILLERT, *Acta Metall.* **36** (1988) 3177.

Received 4 April
and accepted 30 July 1991